Dendritic coding of multiple sensory inputs in single cortical neurons in vivo

Zsuzsanna Varga[1], Hongbo Jia[1], Bert Sakmann[2], and Arthur Konnerth[2]

Institute of Neuroscience and Institute for Advanced Study, Technical University Munich, 80802 Munich, Germany

Contributed by Bert Sakmann, July 29, 2011 (sent for review July 20, 2011)

Single cortical neurons in the mammalian brain receive signals arising from multiple sensory input channels. Dendritic integration of these afferent signals is critical in determining the amplitude and time course of the neurons' output signals. As of yet, little is known about the spatial and temporal organization of converging sensory inputs. Here, we combined in vivo two-photon imaging with whole-cell recordings in layer 2 neurons of the mouse vibrissal cortex as a means to analyze the spatial pattern of subthreshold dendritic calcium signals evoked by the stimulation of different whiskers. We show that the principle whisker and the surrounding whiskers can evoke dendritic calcium transients in the same neuron. Distance-dependent attenuation of dendritic calcium transients and the corresponding subthreshold depolarization suggest feed-forward activation. We found that stimulation of different whiskers produced multiple calcium hotspots on the same dendrite. Individual hotspots were activated with low probability in a stochastic manner. We show that these hotspots are generated by calcium signals arising in dendritic spines. Some spines were activated uniquely by single whiskers, but many spines were activated by multiple whiskers. These shared spines indicate the existence of presynaptic feeder neurons that integrate and transmit activity arising from multiple whiskers. Despite the dendritic overlap of whisker-specific and shared inputs, different whiskers are represented by a unique set of activation patterns within the dendritic field of each neuron.

excitatory synapse in vivo | cortical circuits | mouse barrel cortex

Cortical function relies on the network properties of connected neurons. In addition to conventional (1) and modern (2–4) structural reconstructions, electrophysiological (5, 6) and optical tools (7–10) are commonly applied to probe the functional connectivity among neurons. Recent advances in two-photon calcium imaging enabled an in vivo analysis of the dendritic organization of sensory inputs to layer 2/3 neurons in the mouse visual cortex (11). The sensory input sites were represented by local dendritic calcium influx through NMDA receptors called hotspots. The fine structure of the hotspots, whether they represented individual spines or small spinodendritic segments, was not determined. A major finding was that synaptic inputs sharing the same orientation preference are widely distributed throughout the dendritic field, and importantly, inputs with different orientation preference are interspersed. An important open question is whether the presence of such inputs with multiple orientations is related to the fact that, in the mouse visual cortex, neurons selective to different orientations are interspersed (12) rather than being organized into cortical columns. It has been suggested that, in the cat and in primates, the input connection scheme would be differently organized (13), because neurons with different orientation preferences are quite strictly clustered into orientation columns (14). It is, thus, unclear how in vivo inputs are organized on the dendrites of single cortical neurons residing in a column-structured region.

A study by Jia et al. (11) on dendritic organization of inputs in the mouse visual cortex had focused on the signals arising through a single input channel (i.e., a single eye). However, sensory systems generally integrate information from multiple peripheral anatomical input channels (15). For example, the rodent vibrissal cortex integrates information arising from multiple whiskers. It is a widely used model system for studying the function of cortical columns because of the precise relationship between barrels, which are easily visualized through histological staining, and the functional representation of single whiskers (16). However, the representation of whiskers by single barrels is not exclusive. In fact, neurons in a single barrel column can have a subthreshold receptive field comprising several whiskers (17–26). For example, layer 2/3 neurons respond to the stimulation of the principle whisker (PW) and multiple surround whiskers (SW) (27). In addition, stimulation of a single whisker results in a spread of activation through large areas of the barrel cortex (28, 29).

In this study, we investigated how inputs reaching layer 2/3 through two different cortical columns are represented on the dendrites of single layer 2 neurons. We analyzed the distance dependence of changes in subthreshold membrane potential and global dendritic calcium signaling on SW stimulation. We compared the number, spatial distribution, and response probability of input sites activated by stimulation of PW and SW. We applied a similarity-based classifier to distinguish the activation patterns of each trial. Furthermore, we used high-resolution imaging on short dendritic segments to study the fine structure of dendritic input sites down to the single spine level.

Results

Spatial and Temporal Organization of Dendritic Hotspots. We investigated the functional properties of layer 2 neurons with combined whole-cell recordings and two-photon dendritic calcium imaging in the vibrissal cortex of mice in vivo (Fig. 1*A*). Two whiskers in different configurations (C2 and E2, D2, C4, or C1) were spared, whereas all others were acutely trimmed. The topographically related cortical columns for the spared whiskers were located by intrinsic signal optical imaging (30) (Fig. 1*B*). We made targeted whole-cell recordings from neurons in the C2 whisker-related column. Thus, with reference to the neuron, C2 was denoted as the PW, and the other whisker was denoted as the SW. For each recorded neuron, two-photon calcium imaging was performed in 6–11 focal planes (Fig. 1*C*) (31), covering a substantial fraction of dendrites (up to 20–30% of the dendritic tree) (Fig. 1*D*). During combined two-photon calcium imaging and recordings of subthreshold responses, neurons were prevented from action potential firing, if necessary, by slightly hyperpolarizing the membrane potential (about 2–10 mV). Importantly, even with the hyperpolarization, the membrane potentials were in the normal range of resting potentials that are encountered in neurons of layer 2/3 in the rodent barrel cortex (−85 to −60 mV) (32).

Author contributions: Z.V., H.J., B.S., and A.K. designed research; Z.V., H.J., and A.K. performed research; Z.V., H.J., B.S., and A.K. analyzed data; and Z.V., H.J., B.S., and A.K. wrote the paper.

The authors declare no conflict of interest.

[1]Z.V. and H.J. contributed equally to this work.

[2]To whom correspondence may be addressed. E-mail: bs@mpimf-heidelberg.mpg.de or arthur.konnerth@lrz.tum.de.

This article contains supporting information online at www.pnas.org/lookup/suppl/doi:10.1073/pnas.1112355108/-/DCSupplemental.

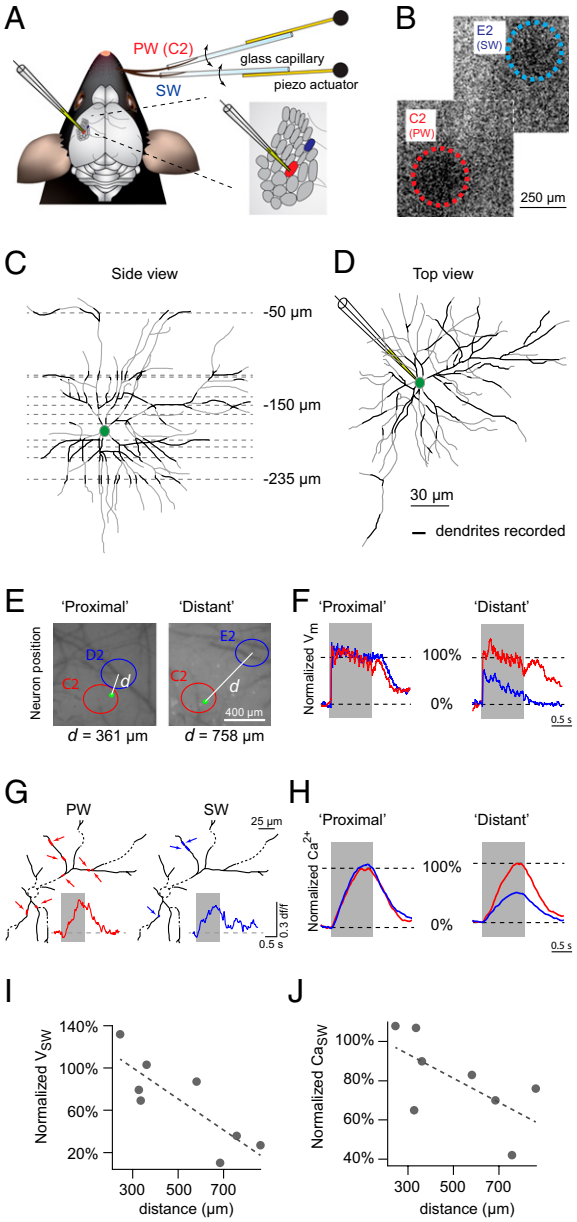

Fig. 1. In vivo two-photon imaging of whisker stimulation-evoked subthreshold dendritic calcium signals. (*A*) Overview of the experiment design. (*B*) Intrinsic signal optical imaging to locate whisker-related columns. The map is a montage of two intrinsic optical images. (*C*) Side view of a level 2/3 neuron. Black lines indicate dendrites recorded with calcium imaging, and dashed lines indicate depth of focal planes. (*D*) Top view of the same neuron as in *C*. (*E*) Example neurons with different distances from the SW column center. Red and blue circles represent PW and SW columns, respectively; the green dot indicates a neuron, and the white line (*d*) indicates the distance between the neuron and SW column. (*F*) Whisker stimulation-evoked average (n = 100) subthreshold depolarization normalized to the average value of PW response (absolute mean amplitude for proximal = 3.9 mV, absolute mean amplitude for distant = 4.2 mV). Red and blue traces represent PW- and SW-evoked responses, respectively; gray shading indicates stimulation time window. Traces are from the same neurons as in *E*. The same notations apply for *G* and *H*. (*G*) Examples of PW- and SW-evoked dendritic calcium signals. Arrows indicate calcium signaling sites, and dashed lines indicate dendritic portions out of the focal plane. (*H*) Normalized global dendritic calcium signals of neurons shown in *E*. Note that corresponding recordings in *F* and *H* were obtained simultaneously; both recorded neurons were hyperpolarized by 2 mV to prevent action potential firing. (*I*) Normalized SW-evoked depolarization amplitude plotted against distance. Each point represents one neuron. Dashed line represents linear fitting. (*J*) Normalized SW-evoked global dendritic calcium signal amplitude plotted against distance. Notations are same as in *I*.

In neurons located either proximal or more distal to the SW-related column (Fig. 1*E*), we found that both PW and SW stimulation evoked subthreshold membrane potential depolarization (Fig. 1*F*) and dendritic calcium transients (Fig. 1*G*). To compare whisker-evoked depolarization with the set of inputs arriving at a single neuron, we calculated the global subthreshold dendritic calcium signal from all trials at all focal planes for each whisker (Fig. 1*H*). This global calcium signal represents an integration of dendritic hotspot signals that are activated by sensory stimulation and is a measure of the afferent synaptic input (11). A distant SW evoked a smaller depolarization and smaller global dendritic calcium signal compared with the PW, whereas the responses evoked by a proximal SW were similar to those responses of the PW. This finding suggests that the distance-dependent weakening of SW responses is caused by the gradual reduction in afferent input. To test the generality of this trend, we calculated the relative differences between PW- and SW-evoked depolarizations and dendritic calcium signals for 12 neurons (Fig. 1 *I* and *J*). All variables (distance, depolarization, and dendritic calcium signal) showed significant pairwise correlation (Pearson correlation): depolarization vs. distance ($r = 0.66$, $P = 0.03$), dendritic calcium vs. distance ($r = 0.62$, $P = 0.04$), and depolarization vs. dendritic calcium ($r = 0.62$, $P = 0.03$). Overall, these results suggest an inverse relationship between the SW to PW distance and the strength of SW input to the PW column.

Next, we characterized the individual local dendritic calcium signals (i.e., hotspots) (11) evoked by whisker stimulation. Typically, several dendrites were visible in one focal plane (Fig. 2*A*), and multiple hotspots were encountered on one dendrite (Fig. 2*B*). To test the response probability of individual hotspots, we examined the same dendritic region repeatedly (Fig. 2*C*). The individual hotspot sites were activated at low probabilities (temporal stochasticity) (Fig. 2 *D* and *E*) and with different patterns of hotspot distribution across trials (spatial stochasticity). We found that the response probability distributions for PW- and SW-evoked hotspots were similar (Fig. 2*F*).

To compare the PW- and SW-evoked patterns, we mapped all hotspot sites weighted with their response probabilities in each focal plane for PW and SW trials separately (Fig. 3 *A* and *B*). Then, the PW- and SW-evoked patterns were superimposed, and therefore, PW- and SW-specific hotspot sites were distinguished. Surprisingly, a large fraction of hotspot sites were shared (activated by both whiskers) (Fig. 3*C*), especially when the SW column was located at a short distance from the recorded neuron (Fig. 3 *D* and *E*).The whisker-specific and shared hotspot sites were intermingled. However, the number of both SW-specific and shared hotspot sites decreased with the distance between the neuron and the SW-related column center (Fig. 3 *D* and *E*) (the Pearson correlation coefficients for number of hotspots vs. distance were PW-specific: $r = 0.26$, $P = 0.42$; SW-specific, $r = -0.72$, $P = 0.008$; shared, $r = -0.72$, $P = 0.009$).

Distinct Sets of Input Patterns of Different Whiskers in Single Neurons. In view of the low probability and stochastic activation pattern of specific and shared input sites, we wondered whether PW or SW stimulation produced whisker-specific input patterns during each single trial. To address this issue, we devised a simple classifier to compare dendritic activation patterns without bias. For this purpose, the raw two-photon images were convolved with spatial and temporal filters and transformed into a new sequence of $\Delta f/f$ images representing the relative fluorescence change of each pixel (*SI Materials and Methods, Data Analysis*). A threshold-based event detector screened the $\Delta f/f$ images, registered the hotspot

NEUROSCIENCE

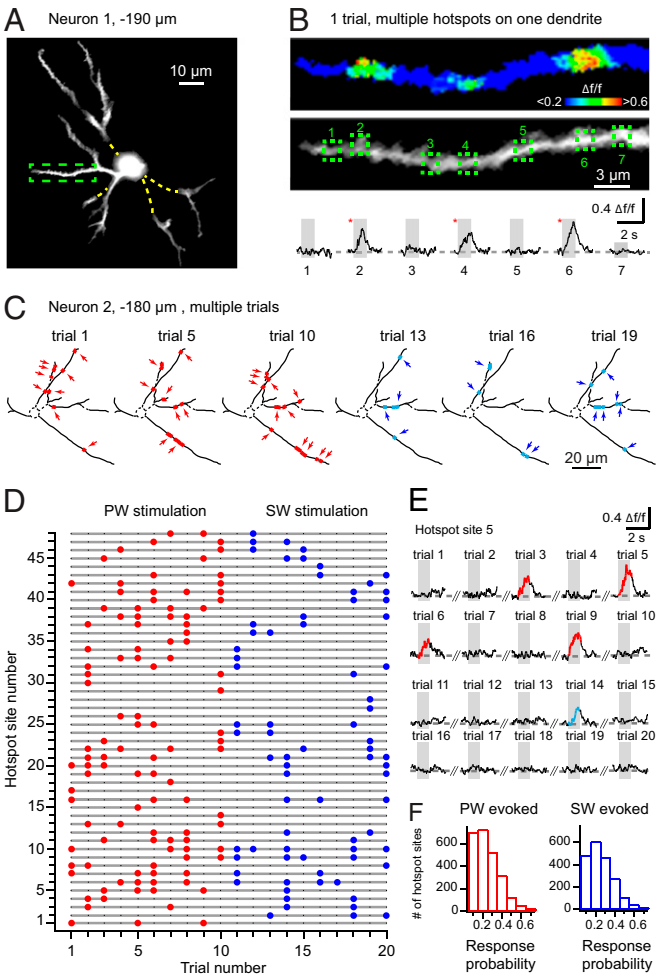

Fig. 2. Spatial and temporal organization of dendritic calcium hotspots. (*A*) Two-photon image of a layer 2 neuron (Alexa channel, average of 280 frames). Yellow dashed lines represent dendrites out of focus, and the green dashed box indicates the dendrite shown in *B*. (*B Top*) Pseudocolor image of the relative fluorescent change in the Oregon Green channel of the dendrite marked in *A* (projection of 1 s). (*B Middle*) Average grayscale image of 280 frames in the Oregon Green channel. Green dashed boxes are regions of interest (ROIs) on the dendrite. (*B Bottom*) Calcium transients calculated from the ROIs indicated in *Middle*. Red asterisks indicate ROIs activated by stimulation, and gray shading represents the stimulation time window. (*C*) Examples of dendritic hotspot activation patterns for 3–3 trials evoked by PW and SW stimulation. Red and blue dots highlighted by arrows represent hotspot sites activated by PW and SW, respectively. (*D*) Graph of the active hotspot sites in the same focal plane as *C*. Red and blue dots indicate hotspots sites activated by the PW and SW, respectively. (*E*) Example of whisker-evoked calcium signals in consecutive trials. Red and blue traces represent calcium transients evoked by PW and SW, respectively; gray shading represents stimulation time window. (*F*) Histograms of the response probability for all hotspots sites in all neurons.

events, and projected the pixels onto one binary image defining the activation pattern of this trial. Using normalized image cross-correlation, we then calculated the correlation coefficient between any two trials of the same focal plane (Fig. S1*A* and *SI Materials and Methods*, *Data Analysis*). We refer to this coefficient as the similarity index, which is in line with the terminology used in automated pattern recognition (33). Fig. 3*F* illustrates the results obtained from a single neuron and shows that the similarity indices among trials of the same whisker were higher (33.6 ± 0.3%, n = 1,620) than among trials of different whiskers (28.3 ± 0.3%, n = 900, unpaired t test, $P < 0.0001$). Similar results were obtained for all 12 neurons (Fig. 3*G*), regardless of their distance to the SW barrel center (each shows a significant difference of $P < 0.0001$). For a given trial, the mean PW similarity or mean SW similarity was defined as the average of similarity indices between the trial and all other PW or SW trials, respectively. The classifier can distinguish between PW and SW trials by judging whether the mean PW similarity value was higher or lower than the mean SW similarity value. Such a correct judgment of a trial means that, in Fig. 3 *F* and *G*, a blue dot is above the diagonal line or a red dot is below the diagonal line. For many focal planes, the classifier performed well above chance level (Fig. S1*B*), with a cumulative success rate of more than 90% over the whole dataset. These results indicate that different whiskers had distinct sets of dendritic activation patterns. In a detailed numerical model (*SI Results* and Figs. S2–S6), we generalized this observation for an indefinite number of trials. The model also predicts that our limited number of trials (10 for each whisker) were sufficient for the classifier to correctly distinguish the two sets of dendritic activation patterns evoked by PW and SW stimulation.

Multiple Input Channels Converge on Single Spines. What is the fine anatomical structure of the shared dendritic hotspots? We considered two alternative hypotheses; first, separate inputs from the PW and a SW may contact distinct nearby spines on the same dendrite, or second, the same spines may be activated by both the PW and at least one SW. Although our initial procedure of in vivo dendritic imaging was useful for monitoring local signaling in larger dendritic fields (11, 31), it did not provide sufficient digital image resolution to resolve these issues. For higher-resolution recordings of whisker stimulation-evoked calcium transients, we used the low-power temporal oversampling (LOTOS) procedure that involves imaging at high-frame rates (200 Hz) and lower excitation intensity per frame (*SI Materials and Methods*, *Two-Photon Calcium Imaging of Spines*) (34). With LOTOS, which helps to reduce photodamage when imaging at high-zoom factors, we were able to image portions (10–20 µm) of spiny dendrites (Fig. 4 *A*–*C*) and record whisker stimulation-evoked calcium transients during repeated trials (Fig. 4 *D* and *E*). The recordings revealed calcium transients in single spines, with small or absent signals in the parent dendritic shaft (Fig. 4 *D* and *E* and Fig. S7). Importantly, the recordings showed that, in addition to whisker-specific spines, some spines were reliably activated by both whiskers (Fig. 4 *E* and *F*), providing direct support for our second hypothesis that the same spines can be activated by both PW and SW.

Discussion

In this study, we combined two-photon calcium imaging and whole-cell recording in vivo to examine the dendritic activation patterns in single neurons of the vibrissal cortex when activating distinct whiskers. From previous studies, it is known that the receptive field of single layer 2 neurons comprises not only the PW but also multiple SWs (24). However, the electrical responses evoked by SW stimulation decrease as the distance between SW and PW increases (27, 29). When analyzing subthreshold dendritic calcium transients representing synaptic input sites, we also found that dendritic calcium responses evoked by SW stimulation decrease as the distance between SW and PW increases. Thus, our results suggest that the distance-dependent attenuation of electrical responsiveness is supported by a feed-forward connection scheme with a likely contribution of inhibitory inputs (35–37).

The whisker stimulation-evoked local dendritic calcium signals (hotspots) found in this study shared similarities with the previously reported dendritic hotspots found in visual cortex (11). In general, however, the density of hotspots on a dendrite that were activated by the stimulation of a whisker was substantially higher than in dendrites of visual cortex neurons when activated by a specific stimulus feature, such as a particular direction of a drifting

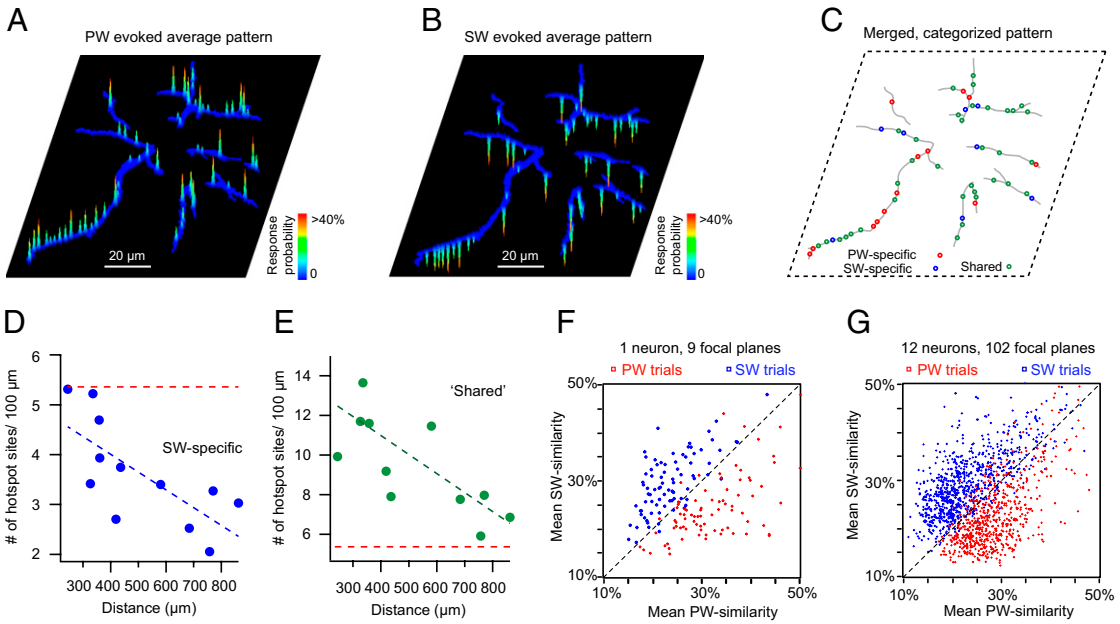

Fig. 3. Distinct dendritic representation of multiple whiskers through specific and shared hotspot sites. (*A* and *B*) Weighted mapping of PW- (*A*) and SW- (*B*) evoked hotspot sites in the same focal plane. Color-coded peaks and valleys represent the response probability of hotspot sites for PW and SW stimulation, respectively. (*C*) Merged mapping of PW-specific (red), SW-specific (blue), and shared (green) hotspot sites. (*D* and *E*) The number of SW-specific (*D*) and shared (*E*) hotspot sites depends on the distance between the neuron and the SW column. Each point represents one neuron. Blue and green dashed lines are linear fitting of the number of SW-specific and shared hotspot sites vs. distance, respectively. The red dashed line represents the average number of PW-specific hotspot sites (the correlation between the number of PW-specific hotspot sites and distance was not significant). (*F* and *G*) Intertrial pattern correlation for all focal planes in one neuron (*F*) and in all 12 neurons (*G*). Each point represents one trial, where the *x* coordinate is the average of pattern correlation value to all of the other PW trials of the same focal plane and the *y* coordinate is the average of pattern correlation value to all of the other SW trials. The dashed line represents the criterion of judgment for the classifier.

grating stimulation. This difference may result from the difference in the mode of sensory stimulation. A remarkable feature of the dendritic organization of hotspots in the dendrites of layer 2 vibrissal cortex neurons was that most individual input sites were activated at low probability for both PW and SW stimulation. The resonant scanner-based two-photon imaging approach used in this study allowed the simultaneous imaging of hotspots in several dendrites across a relatively large field of view. However, spine imaging requires high-zoom factors, and furthermore, image acquisition at high frame rates (200 frames/s in our case) at a reduced excitation power (details on the LOTOS procedure in *Materials and Methods* and ref. 34) is required. Because the speed of the scanning laser beam cannot be increased in a resonant scanner-based system, this finding led to an additional reduction of the effective field of view, such that, in practice, only segments of spiny dendrites of up to 10–20 µm length were used for spine imaging. The whisker-evoked calcium transients recorded in such spiny dendrites showed that the largest calcium transients occurred invariably in spines, with significantly smaller contributions in the adjacent dendritic shafts. In fact, in about two-thirds of the local response, calcium signaling was exclusively detected in the spines but not the adjacent dendrite (Fig. S7). These results do not provide support for the generation of local dendritic regenerative events like dendritic spikes (38). Instead, they indicate that the computational units (39) of dendrites are single active spines. These recordings, however, do not exclude the possibility that, during other conditions of sensory activation (e.g., active whisking in awake animals), this type and other types of cortical neurons (e.g., the large layer 5 pyramidal cells), have different signaling modes in their dendrites, especially in the remote apical tufts (40).

The results show that spines in the same neuron were activated either by the PW or a SW. However, a surprising observation was that some of the spines were activated by both whiskers. The identification of such shared synaptic input sites strongly suggests the existence of intermediary feeder neurons that are capable of firing action potentials in response to both PW and SW stimulation. Based on previous anatomical studies (5, 41), it seems that layer 2/3 pyramidal neurons represent a major fraction of these feeder neurons (Fig. 4*L*). Furthermore, action potential activity in layer 2/3 neurons is typically evoked by both PW and SW deflection (21, 27, 42). In fact, the number of action potentials evoked by proximal SW deflection can be almost as high as the number evoked by PW deflection. Moreover, action potential numbers fall off gradually with deflection of the more distant SWs (27). Additional support for an involvement of layer 2/3 neurons, known to be strongly interconnected with each other (5, 6), comes from our own recordings showing that each recorded neuron received strong inputs from both the PW and the SW and therefore, could act itself as a feeder neuron. Furthermore, smaller contributions may come from neurons with multiwhisker receptive fields that are located in other cortical layers. Such neurons have been found in layer 4 (17–22, 24), layer 5B, and to a lesser extent, layer 5A (23–25). For simplicity, in our model, we considered only the presumably strongest input, which arises from layer 2/3 neurons.

In conclusion, in contrast to the topographically well-organized macroscopic cellular structure of barrel columns, we found that the dendritic organization of single spine synaptic inputs is surprisingly unstructured, with a salt and pepper-like distribution of intermingled inputs from multiple whiskers impinging on the same dendrites. On a trial by trial basis, most of the functional input sites were activated randomly at low probabilities. However, when viewing the pool of dendritic inputs as an ensemble, the set of activation patterns were distinct for different whiskers. Taken together, our results provide basic insights into the dendritic ar-

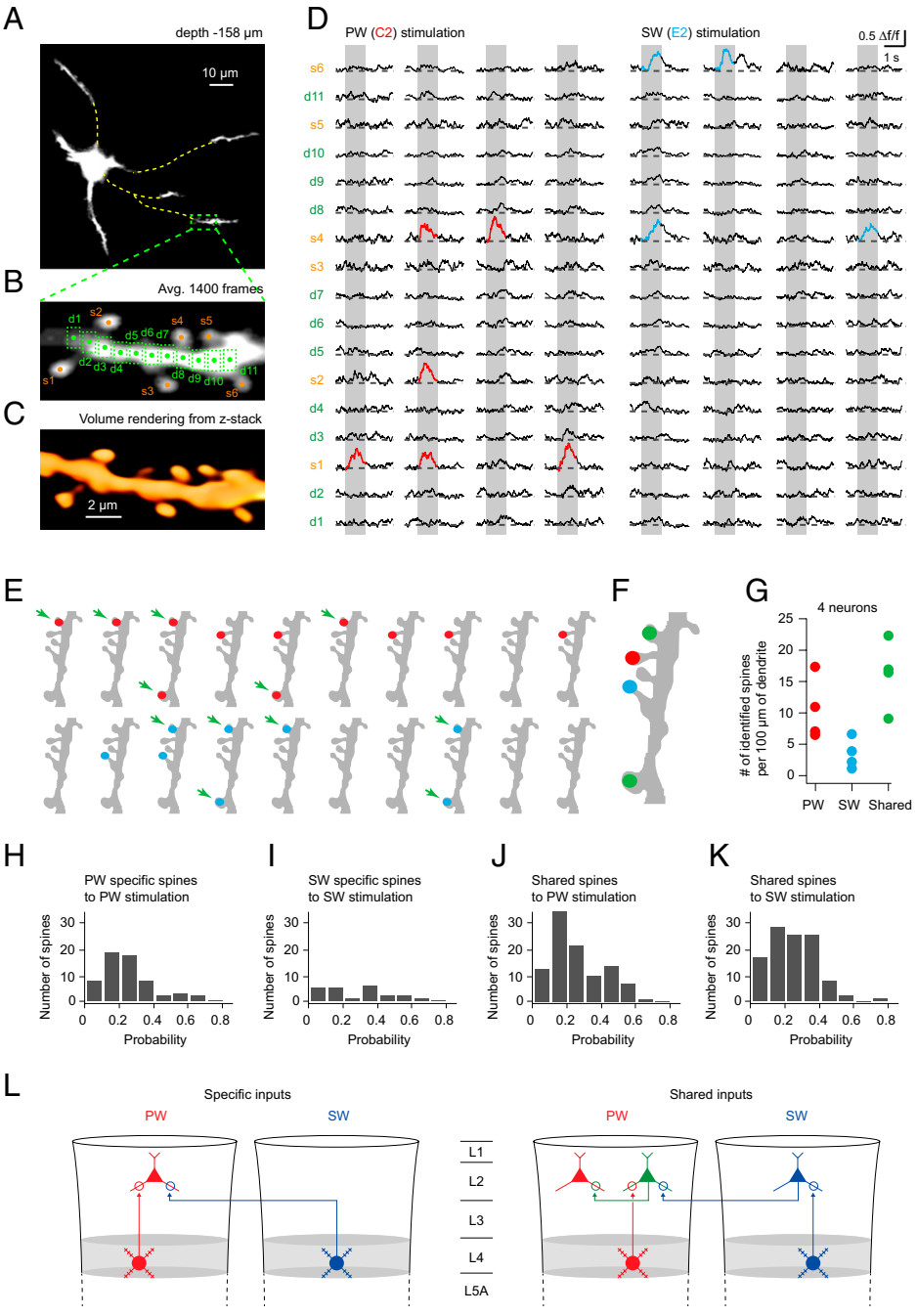

Fig. 4. Multiple peripheral sensory input channels converge on single shared spines. (*A*) Two-photon image of a layer 2 neuron that was recorded in full frame at 40 Hz and averages 280 frames. Yellow dashed lines represent dendrites out of focus, and the green dashed box indicates the portion of dendrite shown in *B*. (*B*) Two-photon image of a dendrite portion (average of 1,400 frames) recorded in partial frame at 200 Hz (*Materials and Methods*). Green boxes with dots and orange dots indicate dendritic segments and spines from which calcium signals were calculated, respectively. (*C*) Top view of the volume rendering of the same dendrite. (*D*) Calcium signals from single spines and dendritic segments as marked in *B*. Red and blue traces represent identified calcium transients in spines evoked by PW and SW, respectively; gray shading represents stimulation time window. (*E*) Spine activation patterns in consecutive trials. Red and blue dots indicate spines activated by PW and SW, respectively; green arrows indicate spines activated by both whiskers. (*F*) Categorization of the spines in *E*. Red, PW-specific; blue, SW-specific; green, shared. (*G*) Number of responsive spines per dendrite length. (*H–K*) Histograms of the response probability of spines in different categories. (*L*) Scheme of the candidate presynaptic sources of PW-specific, SW-specific, and shared inputs.

rangement of sensory signals arising from different input channels onto single neurons of a column-organized cortical region.

Materials and Methods

Animals. All experimental procedures were performed in accordance with institutional animal welfare guidelines and were approved by the state government of Bavaria, Germany. C57BL/6 mice (P28–P38, n = 16) were used for in vivo dendrite and spine imaging experiments. Animal preparation procedures were the same as those procedures previously described (31), except for the treatment of whiskers. With the exception of two whiskers (C2 and E2, D2, C4, or C1) on the right side, all other whiskers were plucked. The spared whiskers were shortened to 1 cm and were inserted into two glass capillaries that could be separately deflected by piezoelectric actuators to ~30° in the rostrocaudal direction. For each trial, a pulse stimulator (Model 2100; A-M systems) delivered a train of voltage pulses (10 pulses, 50 ms, 10 Hz) driving the piezoelectric actuators. In each trial, only one whisker was stimulated.

Intrinsic Signal Optical Imaging. The location of the barrel columns related to the spared whiskers was mapped on the cortex by intrinsic signal optical imaging through the intact skull. Images were acquired at 10 Hz by a custom-made system. Each image was spatially filtered by a Gaussian kernel of 5 × 5 pixels. Image acquisition protocol consisted of two 1-s acquisition periods that were repeated 10 times. The first acquisition period was just after the offset of whisker stimulation, and the second period (baseline) was at 16 s after the stimulation. Relative reflectance changes were calculated as the summed images acquired during stimulation divided by the summed baseline images. The two whiskers were mapped in consecutive sessions.

Whole-Cell Recording. Having the two whisker-related barrels mapped by intrinsic signal optical imaging, whole-cell configuration was established on a layer 2 neuron in one of the barrel columns [principle whisker (C2) -related barrel]. Patch pipettes with resistances of 5–8 MΩ were pulled from borosilicate glass capillaries on a vertical puller (PC-10; Narishige). The pipette solution contained 112 mM K-gluconate, 10 mM Hepes, 8 mM KCl, 10 mM

Na-phosphocreatine, 4 mM Mg-ATP, 0.3 mM Na_2-GTP, 100 μM Oregon Green 488 BAPTA-1 hexapotassium salt (OGB1), and 25 μM Alexa Fluor 594 hydrazide sodium salt (Alexa). Current clamp recordings were acquired with an EPC-9 HEKA amplifier using the software package Pulse. Signals were filtered at 3 kHz and digitized at 10 kHz. Series resistances ranged from 20 to 60 MΩ. The exact location of the neuron was determined posthoc by epifluorescence imaging and marked on the map of barrels aligned on the blood vessels (Fig. 1*E*).

Two-Photon Calcium Imaging of Dendritic Hotspots and Spines. Two-photon calcium imaging was performed on a custom-built setup that was similar to the setup used in a previous study (11). A resonant scanner unit (GSI Lumonics), including one fast axis of a 12-kHz resonant mirror and one slow axis of a standard galvanometric mirror, was mounted on an upright microscope chassis (BX51; Olympus) with a long working distance water-immersion objective (40×/0.8; Nikon). Fluorescent excitation light was delivered by a pulsing infrared laser (wavelength = 800 nm, pulse width = 100 fs, repetition rate = 80 MHz) equipped with a prechirper (model DeepSee; Spectra-Physics). Laser power under the objective was typically 30–40 mW and 15–25 mW during dendritic hotspot and spine imaging, respectively. Full-frame images consisted of 512 lines, and they were scanned with a 40-Hz repetition rate. For dendritic hotspot imaging, neurons were imaged in 6–11 focal planes distributed across the whole depth of the dendritic tree. The actual width of the field of view, controlled by the amplitude of scanning mirror rotation, ranged between 80 and 250 μm, depending on the layout of dendrites in the focal plane. For spine imaging, we used the LOTOS procedure (34). The scanner was configured for the following mode: the number of lines was reduced to 64, the number of pixels in each line was reduced to 256, and the image repetition rate was increased to 200 Hz. The width of the field of view was accordingly reduced to the range of 27–42 μm. Each focal plane was probed with 10 trials of PW stimulation and 10 trials of SW stimulation. Trials were interlaced (five PW trials followed by five SW trials that were repeated two times) with variable time intervals (10–20 s) between two consecutive trials. For display purposes (Fig. 2 *C*–*E*) and spines (Fig. 4 *D* and *E*), the trials with the same whisker stimulation were grouped together. *z*-Stack images of the neurons were taken at the largest possible field of view (300 × 300 μm), with a step size of 0.5 μm. *z*-Stack images of spines were taken with the reduced field of view and a step size of 0.2 μm.

Data Analysis. The structural reconstruction was performed using the WCIF-ImageJ software (open access from http://www.uhnresearch.ca/facilities/wcif/imagej/), the whole-cell recordings were analyzed in Igor (Igor Pro v5.0.1.0; Wavemetrics), and the calcium imaging recordings were analyzed by custom-written programs in LabVIEW (version 2009; National Instruments). Statistical tests were performed in SPSS (version 17.0; IBM). *z*-Stack images of spines were deconvolved in Huygens (version J27.14; Scientific Volume Imaging BV), and volume was rendered in Amira (version 5.3.3; Visage Imaging). A detailed description of the algorithms used in the data analysis is in *SI Materials and Methods*.

ACKNOWLEDGMENTS. We thank Jia Lou for excellent technical assistance. We thank Drs. Fitzpatrick, Schummers, Christie, Nelken, and Hill for critically reading early versions of our manuscript. This work was supported by the Deutsche Forschungsgemeinschaft (International Research Training Group 1373), the European Research Area-Net Program, the Center for Integrated Protein Science Munich, and the Schiedel Foundation.

1. Cajal SRY (1994) *Histology of the Nervous System of Man and Vertebrates* (Oxford University Press, London).
2. Lichtman JW, Livet J, Sanes JR (2008) A technicolour approach to the connectome. *Nat Rev Neurosci* 9:417–422.
3. Denk W, Horstmann H (2004) Serial block-face scanning electron microscopy to reconstruct three-dimensional tissue nanostructure. *PLoS Biol* 2:e329.
4. DeFalco J, et al. (2001) Virus-assisted mapping of neural inputs to a feeding center in the hypothalamus. *Science* 291:2608–2613.
5. Feldmeyer D, Lübke J, Sakmann B (2006) Efficacy and connectivity of intracolumnar pairs of layer 2/3 pyramidal cells in the barrel cortex of juvenile rats. *J Physiol* 575:583–602.
6. Lefort S, Tomm C, Floyd Sarria JC, Petersen CC (2009) The excitatory neuronal network of the C2 barrel column in mouse primary somatosensory cortex. *Neuron* 61:301–316.
7. Boyden ES, Zhang F, Bamberg E, Nagel G, Deisseroth K (2005) Millisecond-timescale, genetically targeted optical control of neural activity. *Nat Neurosci* 8:1263–1268.
8. Nikolenko V, Poskanzer KE, Yuste R (2007) Two-photon photostimulation and imaging of neural circuits. *Nat Methods* 4:943–950.
9. Petreanu L, Mao T, Sternson SM, Svoboda K (2009) The subcellular organization of neocortical excitatory connections. *Nature* 457:1142–1145.
10. Shepherd GM, Svoboda K (2005) Laminar and columnar organization of ascending excitatory projections to layer 2/3 pyramidal neurons in rat barrel cortex. *J Neurosci* 25:5670–5679.
11. Jia H, Rochefort NL, Chen X, Konnerth A (2010) Dendritic organization of sensory input to cortical neurons in vivo. *Nature* 464:1307–1312.
12. Ohki K, Reid RC (2007) Specificity and randomness in the visual cortex. *Curr Opin Neurobiol* 17:401–407.
13. Priebe NJ, Ferster D (2010) Neuroscience: Each synapse to its own. *Nature* 464: 1290–1291.
14. Hubel DH, Wiesel TN (1962) Receptive fields, binocular interaction and functional architecture in the cat's visual cortex. *J Physiol* 160:106–154.
15. Celikel T, Sakmann B (2007) Sensory integration across space and in time for decision making in the somatosensory system of rodents. *Proc Natl Acad Sci USA* 104:1395–1400.
16. Woolsey TA, Van der Loos H (1970) The structural organization of layer IV in the somatosensory region (SI) of mouse cerebral cortex. The description of a cortical field composed of discrete cytoarchitectonic units. *Brain Res* 17:205–242.
17. Armstrong-James M, Callahan CA (1991) Thalamo-cortical processing of vibrissal information in the rat. II. Spatiotemporal convergence in the thalamic ventroposterior medial nucleus (VPm) and its relevance to generation of receptive fields of S1 cortical "barrel" neurones. *J Comp Neurol* 303:211–224.
18. Armstrong-James M, Callahan CA, Friedman MA (1991) Thalamo-cortical processing of vibrissal information in the rat. I. Intracortical origins of surround but not centre-receptive fields of layer IV neurones in the rat S1 barrel field cortex. *J Comp Neurol* 303:193–210.
19. Armstrong-James M, Fox K, Das-Gupta A (1992) Flow of excitation within rat barrel cortex on striking a single vibrissa. *J Neurophysiol* 68:1345–1358.
20. Brecht M, Sakmann B (2002) Dynamic representation of whisker deflection by synaptic potentials in spiny stellate and pyramidal cells in the barrels and septa of layer 4 rat somatosensory cortex. *J Physiol* 543:49–70.
21. de Kock CP, Bruno RM, Spors H, Sakmann B (2007) Layer- and cell-type-specific suprathreshold stimulus representation in rat primary somatosensory cortex. *J Physiol* 581:139–154.
22. Hirata A, Castro-Alamancos MA (2008) Cortical transformation of wide-field (multiwhisker) sensory responses. *J Neurophysiol* 100:358–370.
23. Manns ID, Sakmann B, Brecht M (2004) Sub- and suprathreshold receptive field properties of pyramidal neurones in layers 5A and 5B of rat somatosensory barrel cortex. *J Physiol* 556:601–622.
24. Moore CI, Nelson SB (1998) Spatio-temporal subthreshold receptive fields in the vibrissa representation of rat primary somatosensory cortex. *J Neurophysiol* 80:2882–2892.
25. Wright N, Fox K (2010) Origins of cortical layer V surround receptive fields in the rat barrel cortex. *J Neurophysiol* 103:709–724.
26. Zhu JJ, Connors BW (1999) Intrinsic firing patterns and whisker-evoked synaptic responses of neurons in the rat barrel cortex. *J Neurophysiol* 81:1171–1183.
27. Brecht M, Roth A, Sakmann B (2003) Dynamic receptive fields of reconstructed pyramidal cells in layers 3 and 2 of rat somatosensory barrel cortex. *J Physiol* 553:243–265.
28. Kleinfeld D, Delaney KR (1996) Distributed representation of vibrissa movement in the upper layers of somatosensory cortex revealed with voltage-sensitive dyes. *J Comp Neurol* 375:89–108.
29. Petersen CC, Grinvald A, Sakmann B (2003) Spatiotemporal dynamics of sensory responses in layer 2/3 of rat barrel cortex measured in vivo by voltage-sensitive dye imaging combined with whole-cell voltage recordings and neuron reconstructions. *J Neurosci* 23:1298–1309.
30. Grinvald A, Lieke E, Frostig RD, Gilbert CD, Wiesel TN (1986) Functional architecture of cortex revealed by optical imaging of intrinsic signals. *Nature* 324:361–364.
31. Jia H, Rochefort NL, Chen X, Konnerth A (2011) In vivo two-photon imaging of sensory-evoked dendritic calcium signals in cortical neurons. *Nat Protoc* 6:28–35.
32. Svoboda K, Helmchen F, Denk W, Tank DW (1999) Spread of dendritic excitation in layer 2/3 pyramidal neurons in rat barrel cortex in vivo. *Nat Neurosci* 2:65–73.
33. Theodoridis S, Koutroumbas K (2006) *Pattern Recognition* (Elsevier, Amsterdam).
34. Chen X, Leischner U, Rochefort NL, Nelken I, Konnerth A (2011) Functional mapping of single spines in cortical neurons in vivo. *Nature* 475:501–505.
35. Adesnik H, Scanziani M (2010) Lateral competition for cortical space by layer-specific horizontal circuits. *Nature* 464:1155–1160.
36. Derdikman D, Hildesheim R, Ahissar E, Arieli A, Grinvald A (2003) Imaging spatiotemporal dynamics of surround inhibition in the barrels somatosensory cortex. *J Neurosci* 23:3100–3105.
37. Fino E, Yuste R (2011) Dense inhibitory connectivity in neocortex. *Neuron* 69: 1188–1203.
38. Schiller J, Major G, Koester HJ, Schiller Y (2000) NMDA spikes in basal dendrites of cortical pyramidal neurons. *Nature* 404:285–289.
39. Branco T, Häusser M (2010) The single dendritic branch as a fundamental functional unit in the nervous system. *Curr Opin Neurobiol* 20:494–502.
40. Larkum ME, Nevian T, Sandler M, Polsky A, Schiller J (2009) Synaptic integration in tuft dendrites of layer 5 pyramidal neurons: A new unifying principle. *Science* 325: 756–760.
41. Lübke J, Roth A, Feldmeyer D, Sakmann B (2003) Morphometric analysis of the columnar innervation domain of neurons connecting layer 4 and layer 2/3 of juvenile rat barrel cortex. *Cereb Cortex* 13:1051–1063.
42. Kerr JN, et al. (2007) Spatial organization of neuronal population responses in layer 2/3 of rat barrel cortex. *J Neurosci* 27:13316–13328.